Computation of Transmissions and Reflections in Geometrical Optics via the Reduced Liouville Equation *

Shi Jin † and Xin Wen ‡

Abstract

We develop a numerical scheme for the wave front computation of complete transmissions and reflections in geometrical optics. Such a problem can be formulated by a reduced Liouville equation with a discontinuous local wave speed or index of refraction, arising in the high frequency limit of linear waves through inhomogeneous media. The key idea is to incorporate Snell's Law of Refraction into the numerical flux for the reduced Liouville equation. This scheme allows a hyperbolic CFL condition, under which positivity, and stabilities in both l^∞ and l^1 norms, are established. Numerical experiments are carried out to demonstrate the validity and accuracy of this new scheme.

1 Introduction

In this paper, we construct and study a numerical scheme for the reduced Liouville equation in two space dimension:

$$f_t + c(x,y)\cos\theta f_x + c(x,y)\sin\theta f_y + [c_x \sin\theta - c_y \cos\theta]\, f_\theta = 0, \qquad (1.1)$$

*Research supported in part by NSF grant No. DMS-0305080 and NSFC grant for Project 10228101. Wen's research was also supported partially by the Knowledge Innovation Project of the Chinese Academy of Sciences Nos. K5501312S1 and K5502212F1.

†Department of Mathematics, University of Wisconsin, Madison, WI 53706, USA. Email address: jin@math.wisc.edu.

‡Institute of Computational Mathematics, Academy of Mathematics and Systems Science, Chinese Academy of Sciences, P.O.Box 2719, Beijing 100080, China. Email address: wenxin@amss.ac.cn.

where $c(x,y)$ is the local wave speed, $f(t,x,y,\theta)$ is the density distribution of particles depending on position (x,y), time t and the slowness angle $\theta \in (-\pi,\pi]$. We are concerned with the case when $c(x,y)$ contains *discontinuities*, corresponding to different indices of refraction in different media. This discontinuity will generate an *interface*, crossing which waves will undergo transmissions or reflections.

The reduced Liouville equation (1.1) is obtained by using the constant Hamiltonian condition in the 2D full phase space Liouville equation

$$f_t + \frac{c(x,y)\xi}{\sqrt{\xi^2+\eta^2}} f_x + \frac{c(x,y)\eta}{\sqrt{\xi^2+\eta^2}} f_y - c_x\sqrt{\xi^2+\eta^2} f_\xi - c_y\sqrt{\xi^2+\eta^2} f_\eta = 0, \tag{1.2}$$

where (ξ,η) is the slowness vector. The Liouville equation (1.2) is the phase space description of the Hamiltonian system with Hamiltonian

$$H(x,y,\xi,\eta) = c(x,y)\sqrt{\xi^2+\eta^2}. \tag{1.3}$$

In classical mechanics the Hamiltonian (1.3) of a particle remains a constant along the particle trajectory, even when it is being transmitted or reflected by the interface. By using the condition $H \equiv C$ for some constant C, one arrives at the reduced Liouville equation (1.1) which is computationally more efficient.

The Liouville equation (1.2) arises in the phase space description of geometrical optics. It is the high frequency limit of the linear wave equation

$$u_{tt} - c(\mathbf{x})^2 \Delta u = 0, \quad t > 0, \quad \mathbf{x} \in R^2\,. \tag{1.4}$$

Recently several phase space based level set methods are based on the equation (1.2) or (1.1), see [13, 16, 23, 33, 36]. It was used to compute the multivalued phase or velocity beyond caustics. The computations of multivalued solution in geometrical optics, or more generally for nonlinear PDEs, have been an active area of research in recent years, see [2, 3, 5, 4, 8, 15, 10, 11, 13, 12, 18, 19, 16, 24, 37, 41, 6, 36, 23]. However, all these works were developed without the interface. The analytical studies on the geometrical optics limit of linear wave equations through interfaces or solid boundaries were carried out in [1, 32, 39].

In our previous works, we constructed the *Hamiltonian-preserving schemes* that are suitable for the full phase space Liouville equation (1.2) with complete transmissions and reflections [26] or with partial transmissions and reflections [27]. The design principle there was to build the behavior of a particle at the interface–cross over with a changed velocity or/and be reflected with a negative velocity according to a constant Hamiltonian–into the numerical flux. See also earlier works [35, 25]. It gives a selection criterion to select a unique solution, consistent to Snell's Law of Refraction, to the governing equation, which is linearly hyperbolic with singular (discontinuous or measure-valued) coefficients.

When only the wave front is interested one can just use the reduced Liouville equation which reduces the dimension by one. The key idea for the reduced Liouville equation is still to build into the numerical flux the wave behavior at the

interface. This is given by Snell's Law of Refraction. This new, explicit scheme gives a method to select out the physically correct solution for the reduced Liouville equation (1.1) with singular coefficients, and like those in [25, 26], it allows a typical hyperbolic stability condition $\Delta t = O(\Delta x, \Delta y, \Delta\theta)$, under which we also establish the positivity, and l^∞ and l^1 stability for the scheme.

The level set approach developed in [33, 7, 36], by using the reduced Liouville equation, has several advantages such as automatically handling the multivalued wave fronts and controlling the solution resolution. When the wave speed is smooth, the use of a standard finite difference method (SFDM) for the reduced Liouville equation, which is linearly hyperbolic, should be satisfactory. For problems with discontinuous wave speeds, one can still formally use the SFDM by either ignoring or smoothing out the wave speed discontinuities. However, as will be shown by numerical examples in Section 4, the use of the SFDM by ignoring the wave speed discontinuities typically does not lead to physically correct numerical solution that is consistent to Snell's Law. On the other hand, the use of the SFDM by smoothing out the wave speed discontinuities may give convergent solutions, but typically suffers from a severe CFL condition as well as poorer numerical resolution [33, 26]. In [7] the authors take into account the wave reflection into the numerical scheme without considering wave transmission. See also a higher order method able to compute multiple reflections [9]. Such a consideration is suitable for waves hitting a solid wall. However, through an interface, waves can be reflected or transmitted, requiring the numerical scheme to be able to handle both situations. The scheme developed in this paper has such a capability.

We present and validate the scheme in the case of single interface. It can be applied to the case of multiple, isolated interfaces naturally. Moreover, Our idea is not restricted to two space dimension. It can be extended to three space dimension as well. However, as pointed out in [27], its generalization to the case of partial transmissions and reflections at the interface is not straightforward, and will be considered in our future study.

This paper is organized as follows. In Section 2, we present the behavior of waves at an interface (Snell's Law), which guides the design of our scheme. We present the scheme in the simple case of a plane wave hitting a flat interface aligning with the grids. In Section 3 we study its positivity and stability in both l^∞ and l^1 norm. The l^1 stability is established in two space dimension, while in our previous works [26, 27], it was established only in the one space dimension. Numerical examples are given in Section 4 to show the deficiency of the SFDM and the validity and accuracy of the new scheme. We make some concluding remarks in Section 5.

2 The behavior of waves at an interface

In geometrical optics, a wave moving with its density distribution governed by the reduced Liouville equation (1.1) can be transmitted or reflected at an interface. In

two dimensional situation, consider a plane incident wave hitting a vertical interface (see Fig. 2.1). The velocity angle of incident wave denoted by θ_i and of transmitted wave denoted by θ_t obey Snell's Law of Refraction

$$\frac{\sin\theta_i}{c^-} = \frac{\sin\theta_t}{c^+} \tag{2.1}$$

where c^+, c^- indicate the right and left limits of c at the interface. The velocity angle of incident wave and of reflected wave denoted by θ_r obey the reflection law

$$\theta_r = \theta_i \,. \tag{2.2}$$

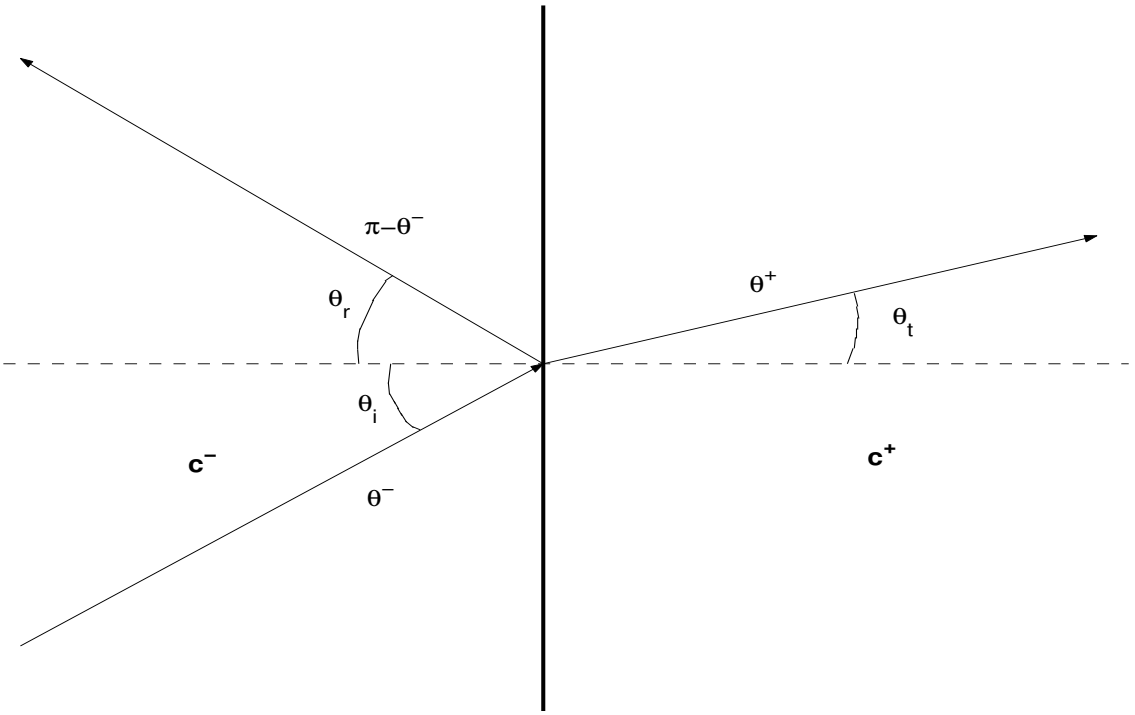

Figure 2.1 Wave transmission and reflection at an interface.

Assume the incident wave has velocity angle θ^- to the left side of the interface, with $0 < \theta^- < \frac{\pi}{2}$. There are two possibilities:

- $|\sin\theta^-|\,\dfrac{c^+}{c^-} < 1$. In this case the wave can transmit through the interface with the new velocity angle

  $$\theta^+ = \arcsin\left(|\sin\theta^-|\,\frac{c^+}{c^-}\right)$$

  obtained using Snell's Law of Refraction (2.1).

- $|\sin\theta^-|\,\dfrac{c^+}{c^-} > 1$. In this case, the wave can not be transmitted and is reflected with the velocity angle $\pi - \theta^-$.

For θ^- in other ranges, similar behavior can also be analyzed using Snell's Law of Refraction (2.1) and the reflection law (2.2).

The solution to the reduced Liouville equation (1.1), which is linearly hyperbolic, can be solved by the method of characteristics. Namely, the density distribution f remains a constant along a bicharacteristics. For a complete transmission or reflection, this implies the following condition at the interface:

$$f(t, x^+, \theta^+) = \begin{cases} f(t, x^-, \theta^-) & \text{transmitted wave} \\ f(t, x^+, \pm\pi - \theta^+) & \text{reflected wave} \end{cases}, \tag{2.3}$$

where θ^- is defined from θ^+ through Snell's Law of Refraction (2.1). The $\pm$ signs in the expression for the reflection case are determined so that $\pm\pi - \theta^+ \in (-\pi, \pi]$. This is the main idea in this paper, used in constructing the numerical flux across the interface in the next section.

3 The numerical scheme and its stability

3.1 The numerical flux

Consider the 2D reduced Liouville equation (1.1). We employ a uniform mesh with grid points at $x_{i+\frac{1}{2}}, y_{j+\frac{1}{2}}, \theta_{k+\frac{1}{2}}$ in each direction. The cells are centered at (x_i, y_j, θ_k) with $x_i = \frac{1}{2}(x_{i+\frac{1}{2}} + x_{i-\frac{1}{2}}), y_j = \frac{1}{2}(y_{j+\frac{1}{2}} + y_{j-\frac{1}{2}}), \theta_k = \frac{1}{2}(\theta_{k+\frac{1}{2}} + \theta_{k-\frac{1}{2}})$, where $i = 1, \cdots, M, j = 1, \cdots, N, k = 1, \cdots, \Theta$. The mesh size is denoted by $\Delta x = x_{i+\frac{1}{2}} - x_{i-\frac{1}{2}}, \Delta y = y_{j+\frac{1}{2}} - y_{j-\frac{1}{2}}, \Delta\theta = \theta_{k+\frac{1}{2}} - \theta_{k-\frac{1}{2}}$. The mesh in θ direction is chosen so that θ_k and $\pm\pi - \theta_k \in (-\pi, \pi]$ are both cell centers for the convenience of implementation. We assume a uniform time step Δt and the discrete time is given by $0 = t_0 < t_1 < \cdots < t_L = T$. We define the cell average of f as

$$f_{ijk} = \frac{1}{\Delta x \Delta y \Delta\theta} \int_{x_{i-\frac{1}{2}}}^{x_{i+\frac{1}{2}}} \int_{y_{j-\frac{1}{2}}}^{y_{j+\frac{1}{2}}} \int_{\theta_{k-\frac{1}{2}}}^{\theta_{k+\frac{1}{2}}} f(x, y, \theta, t) d\theta dy dx.$$

As adopted in [26, 27], we approximate $c(x, y)$ by a piecewise bilinear function, and use the left (c^-) and right (c^+) limits of c at each cell interface. When c is smooth at a cell interface, the two limit values of c coincide. We assume the interface is aligned with the mesh. Define the averaged wave speed in a cell by averaging the four cell interface values

$$c_{ij} = \frac{1}{4}(c^+_{i-\frac{1}{2},j} + c^-_{i+\frac{1}{2},j} + c^+_{i,j-\frac{1}{2}} + c^-_{i,j+\frac{1}{2}}).$$

Then the 2D reduced Liouville equation (1.1) can be semi-discretized as

$$(f_{ijk})_t \quad + \quad \frac{c_{ij}\cos\theta_k}{\Delta x}\left(f^-_{i+\frac{1}{2},jk} - f^+_{i-\frac{1}{2},jk}\right) + \frac{c_{ij}\sin\theta_k}{\Delta y}\left(f^-_{i,j+\frac{1}{2},k} - f^+_{i,j-\frac{1}{2},k}\right)$$

$$+ \quad \left[\frac{c^-_{i+\frac{1}{2},j} - c^+_{i-\frac{1}{2},j}}{\Delta x \Delta\theta} \sin\theta_k - \frac{c^-_{i,j+\frac{1}{2}} - c^+_{i,j-\frac{1}{2}}}{\Delta y \Delta\theta} \cos\theta_k \right] \left(f_{ij,k+\frac{1}{2}} - f_{ij,k-\frac{1}{2}} \right)$$
$$= \quad 0, \tag{3.1}$$

where the interface values $f_{ij,k+\frac{1}{2}}$ are provided by the upwind approximation. The essential part of our algorithm is to define the split numerical fluxes $f^-_{i+\frac{1}{2},jk}$, $f^+_{i-\frac{1}{2},jk}$, $f^-_{i,j+\frac{1}{2},k}$, $f^+_{i,j-\frac{1}{2},k}$ at each cell interface. We will use condition (2.3) to define these fluxes.

Assume c is discontinuous on the mesh interface connected by $(x_{i+\frac{1}{2}}, y_{j-\frac{1}{2}})$ and $(x_{i+\frac{1}{2}}, y_{j+\frac{1}{2}})$. Consider the case $\cos\theta_k > 0$. Using the upwind scheme, $f^-_{i+\frac{1}{2},jk} = f_{ijk}$. However, the flux $f^+_{i+\frac{1}{2},jk}$ should be determined by condition (2.3) by setting $\theta^+ = \theta_k$. Since θ^-_k may not be a grid point, we have to define it approximately. One can first locate the two cell centers that bound θ^-_k, and then use the linear interpolation to evaluate the needed numerical flux at θ^-_k. This corresponds to the strategy adopted in the finite difference version of the method given in [26]. The case of $\cos\theta_k < 0$ is treated similarly. The detailed algorithm to generate the numerical flux is given below.

Algorithm

- if $\cos\theta_k > 0$

  $f^-_{i+\frac{1}{2},jk} = f_{ijk}$,

  ☆ if $\left(|\sin\theta_k| \frac{C^-_{i+\frac{1}{2},j}}{C^+_{i+\frac{1}{2},j}} \right) < 1$

  if $\sin\theta_k \geq 0$

  $\theta^- = \arcsin\left(|\sin\theta_k| \frac{C^-_{i+\frac{1}{2},j}}{C^+_{i+\frac{1}{2},j}} \right)$

  else

  $\theta^- = -\arcsin\left(|\sin\theta_k| \frac{C^-_{i+\frac{1}{2},j}}{C^+_{i+\frac{1}{2},j}} \right)$

  end

  if $\theta_{k'} \leq \theta^- < \theta_{k'+1}$ for some k'

  then $f^+_{i+\frac{1}{2},jk} = \frac{\theta_{k'+1} - \theta^-}{\Delta\theta} f_{ij,k'} + \frac{\theta^- - \theta_{k'}}{\Delta\theta} f_{ij,k'+1}$

  ☆ else

  $f^+_{i+\frac{1}{2},jk} = f_{i+1,j,k'}$ where $\begin{cases} \theta_{k'} = \pi - \theta_k & \text{if } \sin\theta_k \geq 0 \\ \theta_{k'} = -\pi - \theta_k & \text{if } \sin\theta_k < 0 \end{cases}$

  ☆ end

- if $\cos\theta_k < 0$

$f^+_{i+\frac{1}{2},jk} = f_{i+1,jk}$,

☆ if $\left(|\sin\theta_k|\,\frac{C^+_{i+\frac{1}{2},j}}{C^-_{i+\frac{1}{2},j}}\right) < 1$

if $\sin\theta_k \geq 0$

$\theta^- = \pi - \arcsin\left(|\sin\theta_k|\,\frac{C^+_{i+\frac{1}{2},j}}{C^-_{i+\frac{1}{2},j}}\right)$

else

$\theta^- = -\pi + \arcsin\left(|\sin\theta_k|\,\frac{C^+_{i+\frac{1}{2},j}}{C^-_{i+\frac{1}{2},j}}\right)$

end

if $\theta_{k'} \leq \theta^- < \theta_{k'+1}$ for some k'

then $f^-_{i+\frac{1}{2},jk} = \dfrac{\theta_{k'+1}-\theta^-}{\Delta\theta} f_{i+1,j,k'} + \dfrac{\theta^- - \theta_{k'}}{\Delta\theta} f_{i+1,j,k'+1}$

☆ else

$$f^-_{i+\frac{1}{2},jk} = f_{ij,k'} \text{ where } \begin{cases} \theta_{k'} = \pi - \theta_k & \text{if } \sin\theta_k \geq 0 \\ \theta_{k'} = -\pi - \theta_k & \text{if } \sin\theta_k < 0 \end{cases}$$

☆ end

One may sometimes encounter the case when $|\theta^-|$ is close to $\frac{\pi}{2}$ and $|\theta_{k'}|, |\theta_{k'+1}|$ are at the two sides of $\frac{\pi}{2}$. Since f is typically discontinuous at $\theta = \pm\frac{\pi}{2}$ near the wave speed interface, it is not reasonable to interpolate the numerical flux from the cell average of f at $\theta_{k'}, \theta_{k'+1}$. Since this is a rare situation, a simple strategy is to set the numerical flux as the cell average at $\theta_{k'}$ or $\theta_{k'+1}$. For example, in the situation that $\cos\theta_k > 0$, $\theta_{k'} \leq \theta^- < \frac{\pi}{2} < \theta_{k'+1}$, we set $f^+_{i+\frac{1}{2},jk} = f_{ij,k'}$.

The flux $f^\pm_{i,j+\frac{1}{2},k}$ can be constructed similarly.

The above algorithm for evaluating numerical fluxes is of first order. One can obtain a second order flux by incorporating the slope limiter, such as the van Leer or minmod slope limiter [31, 42], into the above algorithm. This can be achieved by replacing $f_{ij,k'}$ with $f_{ij,k'} + \frac{\Delta x}{2} s_{ij,k'}$, and replacing $f_{i+1,j,k'}$ with $f_{i+1,j,k'} - \frac{\Delta x}{2} s_{i+1,j,k'}$ in the above algorithm for all the possible index k', where $s_{ij,k'}$ is the slope limiter in the x-direction.

We remark that the slope limiter near the interface should be modified. Suppose that in a cell centered at (x_i, y_j, θ_k), there is an interface along the cell interface at $x = x_{i-\frac{1}{2}}$, and there is no other vertical interface in the neighborhood. We discuss the modified slope for the x-derivative (if the interface is parallel to the x-axis, then the slope in the y-derivative should be modified similarly). The usual slope limiter in this cell is defined as

$$s_{ijk} = S(f_{i-1,jk}, f_{ijk}, f_{i+1,jk}), \tag{3.2}$$

where S is the slope limiter operator. Since the bicharacteristic is discontinuous at $x_{i-\frac{1}{2}}$, the use of cell average $f_{i-1,jk}$ in the above operator is not appropriate. There are two options:

1) $s_{ijk} = \frac{f_{i+1,jk} - f_{ijk}}{\Delta x}$

2) use the above Algorithm that generates the numerical flux to define the value used in the slope limiter, namely

☆ if $\left(|\sin\theta_k| \frac{C^-_{i-\frac{1}{2},j}}{C^+_{i-\frac{1}{2},j}} \right) < 1$

❑ if $\sin\theta_k \geq 0$, $\cos\theta_k > 0$

$$\theta^- = \arcsin\left(|\sin\theta_k| \frac{C^-_{i-\frac{1}{2},j}}{C^+_{i-\frac{1}{2},j}} \right)$$

❑ if $\sin\theta_k \geq 0$, $\cos\theta_k < 0$

$$\theta^- = \pi - \arcsin\left(|\sin\theta_k| \frac{C^-_{i-\frac{1}{2},j}}{C^+_{i-\frac{1}{2},j}} \right)$$

❑ if $\sin\theta_k < 0$, $\cos\theta_k > 0$

$$\theta^- = -\arcsin\left(|\sin\theta_k| \frac{C^-_{i-\frac{1}{2},j}}{C^+_{i-\frac{1}{2},j}} \right)$$

❑ if $\sin\theta_k < 0$, $\cos\theta_k < 0$

$$\theta^- = -\pi + \arcsin\left(|\sin\theta_k| \frac{C^-_{i-\frac{1}{2},j}}{C^+_{i-\frac{1}{2},j}} \right)$$

❑ end

if $\theta_{k'} \leq \theta^- < \theta_{k'+1}$ for some k'

then set $\widehat{f} = \frac{\theta_{k'+1} - \theta^-}{\Delta\theta} f_{i-1,j,k'} + \frac{\theta^- - \theta_{k'}}{\Delta\theta} f_{i-1,j,k'+1}$

☆ else

$$\text{set } \widehat{f} = f_{ij,k'}, \text{ where } \begin{cases} \theta_{k'} = \pi - \theta_k & \text{if } \sin\theta_k \geq 0 \\ \theta_{k'} = -\pi - \theta_k & \text{if } \sin\theta_k < 0 \end{cases}$$

☆ end

Then set $s_{ijk} = S(\widehat{f}, f_{ijk}, f_{i+1,jk})$.

When the solution to the right hand side of the interface is smooth, the first option is appropriate, while the second option may lead to a loss of accuracy due to the use of the slope limiter on the values at both sides of the interface. However, if there are discontinuities in the solution at the right neighborhood of the interface, the first option is inadequate, and one needs to use the limited slope as in the second option.

According to above analysis, we propose to use a combination of these two options. First, we determine the smoothness of the solution at the right neighborhood

of $x_{i-\frac{1}{2}}$ by checking the ratio $\frac{|f_{i+2,jk}-f_{i+1,jk}|}{|f_{i+1,jk}-f_{ijk}|}$. The cases $f_{ijk}=f_{i+1,jk}$, $f_{i+1,jk}=f_{i+2,jk}$, $\frac{|f_{i+2,jk}-f_{i+1,jk}|}{|f_{i+1,jk}-f_{ijk}|}>D_c$ and $\frac{|f_{i+2,jk}-f_{i+1,jk}|}{|f_{i+1,jk}-f_{ijk}|}<\frac{1}{D_c}$ are classified as the nonsmooth situation, where D_c is a constant slightly larger than 1. Otherwise it is the smooth situation. We then use option 1) for the smooth case and option 2) for the nonsmooth case. In the second option the van Leer limiter is used in our numerical results in Section 4.

After the spatial discretization is specified for (3.1), one can use any time discretization for the time derivative.

3.2 Positivity and l^∞ contraction

Since the exact solution of the reduced Liouville equation is positive when it is initially, it is important that the numerical solution inherits this property.

We only consider the scheme using the first order numerical flux, and the forward Euler method in time. Without loss of generality, we consider the case $\cos\theta_k > 0, \sin\theta_k > 0, c^-_{i+\frac{1}{2},j} < c^+_{i-\frac{1}{2},j}, c^-_{i,j+\frac{1}{2}} < c^+_{i,j-\frac{1}{2}}$ and $T_{ijk} > 0$ for all i,j,k with T_{ijk} defined as

$$T_{ijk}=\frac{c^-_{i+\frac{1}{2},j}-c^+_{i-\frac{1}{2},j}}{\Delta x}\sin\theta_k-\frac{c^-_{i,j+\frac{1}{2}}-c^+_{i,j-\frac{1}{2}}}{\Delta y}\cos\theta_k,$$

the other cases can be treated similarly with the same conclusion. The scheme (3.1) reads

$$\begin{aligned}&\frac{f^{n+1}_{ijk}-f^n_{ijk}}{\Delta t}+\frac{c_{ij}\cos\theta_k}{\Delta x}\left[f_{ijk}-(d_1f_{i-1,j,k'}+d_2f_{i-1,j,k'+1})\right]\\ +\quad&\frac{c_{ij}\sin\theta_k}{\Delta y}\left[f_{ijk}-(d'_1f_{i,j-1,k''}+d'_2f_{i,j-1,k''+1})\right]+\frac{T_{ijk}}{\Delta\theta}\left(f_{ijk}-f_{ij,k-1}\right)=0\end{aligned}$$

where d_1,d_2,d'_1,d'_2 are non-negative and $d_1+d_2=d'_1+d'_2=1$. We omit the superscript n of f. The above scheme can be rewritten as

$$\begin{aligned}f^{n+1}_{ijk}\;=\;&\left(1-c_{ij}\cos\theta_k\frac{\Delta t}{\Delta x}-c_{ij}\sin\theta_k\frac{\Delta t}{\Delta y}-T_{ijk}\frac{\Delta t}{\Delta\theta}\right)f_{ijk}\\ &+c_{ij}\cos\theta_k\frac{\Delta t}{\Delta x}\left(d_1f_{i-1,j,k'}+d_2f_{i-1,j,k'+1}\right)\\ &+c_{ij}\sin\theta_k\frac{\Delta t}{\Delta y}\left(d'_1f_{i,j-1,k''}+d'_2f_{i,j-1,k''+1}\right)\\ &+T_{ijk}\frac{\Delta t}{\Delta\theta}f_{ij,k-1}\,.\end{aligned}\tag{3.3}$$

Now we investigate the positivity of scheme (3.3). This is to prove that if $f^n_{ijk}\geq 0$ for all (i,j,k), then this is also true for f^{n+1}. Clearly one just needs to show that

all the coefficients for f^n are non-negative. A sufficient condition for this is clearly

$$1 - c_{ij}\frac{\Delta t}{\Delta x} - c_{ij}\frac{\Delta t}{\Delta y} - \left(\frac{\left| c^-_{i+\frac{1}{2},j} - c^+_{i-\frac{1}{2},j} \right|}{\Delta x} + \frac{\left| c^-_{i,j+\frac{1}{2}} - c^+_{i,j-\frac{1}{2}} \right|}{\Delta y} \right) \frac{\Delta t}{\Delta \theta} \geq 0,$$

or

$$\Delta t \max_{i,j} \left[\frac{c_{ij}}{\Delta x} + \frac{c_{ij}}{\Delta y} + \frac{1}{\Delta \theta} \left(\frac{\left| c^-_{i+\frac{1}{2},j} - c^+_{i-\frac{1}{2},j} \right|}{\Delta x} + \frac{\left| c^-_{i,j+\frac{1}{2}} - c^+_{i,j-\frac{1}{2}} \right|}{\Delta y} \right) \right] \leq 1. \qquad (3.4)$$

This CFL condition is a hyperbolic one since the quantities $\frac{\left| c^-_{i+\frac{1}{2},j} - c^+_{i-\frac{1}{2},j} \right|}{\Delta x}$ and $\frac{\left| c^-_{i,j+\frac{1}{2}} - c^+_{i,j-\frac{1}{2}} \right|}{\Delta y}$ represent the wave speed gradient at its *smooth* point, which has a *finite* upper bound. Thus our scheme allows a time step $\Delta t = O(\Delta x, \Delta y, \Delta \theta)$.

According to the study in [34], our second order scheme, which incorporates slope adjustment into the first order scheme, is positive under the half CFL condition, namely, the constant on the right hand side of (3.4) is 1/2.

The above conclusion is drawn for the forward Euler time discretization. One can draw the same conclusion for the second order TVD Runge-Kutta time discretization [40].

The l^∞-contracting property of this scheme follows easily, because the coefficients in (3.3) are positive and the sum of them is 1.

3.3 The l^1-stability of the scheme

In this subsection we prove the l^1-stability of the new scheme (with the first order numerical flux and the forward Euler method in time) under a suitable assumption on the initial data. We also present a counter example that shows that violation of this assumption leads to the development of an unbounded numerical solution. Such a property is similar to those proved in [28] for the finite difference version of the Hamiltonian preserving scheme for the Liouville equation with discontinuous potentials. However, in [28] we establish the stability in one space dimension, while here we study it in two space dimension.

We consider the simple case when the interface aligns with a mesh interface at $x_{m+\frac{1}{2}}$, and the wave speed is c^- and c^+ at the left and right hand sides of the interface respectively. Assume $c^- > c^+$. We consider the case that $\pm\frac{\pi}{2}$ are the grid points in θ-direction, and the mesh ratios $\frac{\Delta t}{\Delta x}, \frac{\Delta t}{\Delta y}, \frac{\Delta t}{\Delta \theta}$ are fixed, $O(1)$ numbers.

We define the index set representing the computational domain

$$E_d = \{(i,j,k) | i = 1, \cdots, N, j = 1, \cdots, M, k = 1, \cdots, \Theta\}. \qquad (3.5)$$

Define the l^1-norm of the numerical solution f_{ijk} to be

$$|f|_1 = \frac{1}{N_d} \sum_{(i,j,k)\in E_d} |f_{ijk}|$$

with N_d being the number of elements in E_d.

Given the initial data $f^0_{ijk}, (i,j,k) \in E_d$. Denote the numerical solution at time T to be $f^L_{ijk}, (i,j,k) \in E_d$. To prove the l^1-stability, we need to show that $|f^L|_1 \leq C|f^0|_1$.

Due to the linearity of the scheme, the equation for the error between the analytical and the numerical solution is the same as the scheme itself, so in this section, f_{ijk} will denote the error. We assume there is no error at the boundary, thus $f^n_{ijk} = 0$ at the boundary. If the l^1-norm of the error introduced at each time step in the incoming boundary cells is ensured to be $o(1)$ part of $|f^n|_1$, our following analysis still applies.

Since $c_x = c_y = 0$ at the two sides of $x_{m+1/2}$, the new scheme is given by:

- if $i = m+1, \cos\theta_k > 0$

  1) $\sin\theta_k \geq 0$

     I) $\left(|\sin\theta_k| \frac{c^-}{c^+}\right) < 1$

$$\begin{aligned} f^{n+1}_{m+1,jk} &= \left(1 - c^+\cos\theta_k\frac{\Delta t}{\Delta x} - c^+\sin\theta_k\frac{\Delta t}{\Delta y}\right) f_{m+1,jk} \\ &\quad + c^+\cos\theta_k\frac{\Delta t}{\Delta x}\left(d_{k,k'}f_{mj,k'} + d_{k,k'+1}f_{mj,k'+1}\right) \\ &\quad + c^+\sin\theta_k\frac{\Delta t}{\Delta y}f_{m+1,j-1,k}, \end{aligned} \tag{3.6}$$

$$\text{where} \quad \theta_{k'} \leq \arcsin\left(|\sin\theta_k|\,\frac{c^-}{c^+}\right) < \theta_{k'+1}.$$

     II) $\left(|\sin\theta_k| \frac{c^-}{c^+}\right) \geq 1$

$$\begin{aligned} f^{n+1}_{m+1,jk} &= \left(1 - c^+\cos\theta_k\frac{\Delta t}{\Delta x} - c^+\sin\theta_k\frac{\Delta t}{\Delta y}\right) f_{m+1,jk} \\ &\quad + c^+\cos\theta_k\frac{\Delta t}{\Delta x}f_{m+1,j,k''} \\ &\quad + c^+\sin\theta_k\frac{\Delta t}{\Delta y}f_{m+1,j-1,k}, \end{aligned} \tag{3.7}$$

$$\text{where} \quad \theta_{k''} = \pi - \theta_k.$$

  2) $\sin\theta_k < 0$

     I) $\left(|\sin\theta_k| \frac{c^-}{c^+}\right) < 1$

$$
\begin{aligned}
f_{m+1,jk}^{n+1} &= \left(1 - c^+ \cos\theta_k \frac{\Delta t}{\Delta x} - c^+ \left|\sin\theta_k\right| \frac{\Delta t}{\Delta y}\right) f_{m+1,jk} \\
&\quad + c^+ \cos\theta_k \frac{\Delta t}{\Delta x} \left(d_{k,k'} f_{mj,k'} + d_{k,k'+1} f_{mj,k'+1}\right) \\
&\quad + c^+ \left|\sin\theta_k\right| \frac{\Delta t}{\Delta y} f_{m+1,j+1,k}, \qquad (3.8) \\
&\qquad \text{where} \quad \theta_{k'} \le -\arcsin\left(\left|\sin\theta_k\right| \frac{c^-}{c^+}\right) < \theta_{k'+1}.
\end{aligned}
$$

II) $\left(\left|\sin\theta_k\right| \frac{c^-}{c^+}\right) \ge 1$

$$
\begin{aligned}
f_{m+1,jk}^{n+1} &= \left(1 - c^+ \cos\theta_k \frac{\Delta t}{\Delta x} - c^+ \left|\sin\theta_k\right| \frac{\Delta t}{\Delta y}\right) f_{m+1,jk} \\
&\quad + c^+ \cos\theta_k \frac{\Delta t}{\Delta x} f_{m+1,j,k''} \\
&\quad + c^+ \left|\sin\theta_k\right| \frac{\Delta t}{\Delta y} f_{m+1,j+1,k}, \qquad (3.9) \\
&\qquad \text{where} \quad \theta_{k''} = -\pi - \theta_k.
\end{aligned}
$$

- if $i = m, \cos\theta_k < 0$

1) $\sin\theta_k \ge 0$

$$
\begin{aligned}
f_{mjk}^{n+1} &= \left(1 - c^- \left|\cos\theta_k\right| \frac{\Delta t}{\Delta x} - c^- \sin\theta_k \frac{\Delta t}{\Delta y}\right) f_{mjk} \\
&\quad + c^- \left|\cos\theta_k\right| \frac{\Delta t}{\Delta x} \left(d_{k,k'} f_{m+1,j,k'} + d_{k,k'+1} f_{m+1,j,k'+1}\right) \\
&\quad + c^- \sin\theta_k \frac{\Delta t}{\Delta y} f_{m,j-1,k}, \qquad (3.10) \\
&\qquad \text{where} \quad \theta_{k'} \le \pi - \arcsin\left(\left|\sin\theta_k\right| \frac{c^+}{c^-}\right) < \theta_{k'+1}.
\end{aligned}
$$

2) $\sin\theta_k < 0$

$$
\begin{aligned}
f_{mjk}^{n+1} &= \left(1 - c^- \left|\cos\theta_k\right| \frac{\Delta t}{\Delta x} - c^- \left|\sin\theta_k\right| \frac{\Delta t}{\Delta y}\right) f_{mjk} \\
&\quad + c^- \left|\cos\theta_k\right| \frac{\Delta t}{\Delta x} \left(d_{k,k'} f_{m+1,j,k'} + d_{k,k'+1} f_{m+1,j,k'+1}\right) \\
&\quad + c^- \left|\sin\theta_k\right| \frac{\Delta t}{\Delta y} f_{m,j+1,k}, \qquad (3.11) \\
&\qquad \text{where} \quad \theta_{k'} \le -\pi + \arcsin\left(\left|\sin\theta_k\right| \frac{c^+}{c^-}\right) < \theta_{k'+1}.
\end{aligned}
$$

- if $i \neq m, m+1$

  1) $\cos\theta_k \geq 0, \sin\theta_k \geq 0$

$$\begin{aligned} f_{ijk}^{n+1} &= \left(1 - c_{ij}\cos\theta_k \frac{\Delta t}{\Delta x} - c_{ij}\sin\theta_k \frac{\Delta t}{\Delta y}\right) f_{ijk} \\ &\quad + c_{ij}\cos\theta_k \frac{\Delta t}{\Delta x} f_{i-1,jk} + c_{ij}\sin\theta_k \frac{\Delta t}{\Delta y} f_{i,j-1,k}. \end{aligned} \tag{3.12}$$

  2) $\cos\theta_k \geq 0, \sin\theta_k < 0$

$$\begin{aligned} f_{ijk}^{n+1} &= \left(1 - c_{ij}\cos\theta_k \frac{\Delta t}{\Delta x} - c_{ij}\left|\sin\theta_k\right| \frac{\Delta t}{\Delta y}\right) f_{ijk} \\ &\quad + c_{ij}\cos\theta_k \frac{\Delta t}{\Delta x} f_{i-1,jk} + c_{ij}\left|\sin\theta_k\right| \frac{\Delta t}{\Delta y} f_{i,j+1,k}. \end{aligned} \tag{3.13}$$

  3) $\cos\theta_k < 0, \sin\theta_k \geq 0$

$$\begin{aligned} f_{ijk}^{n+1} &= \left(1 - c_{ij}\left|\cos\theta_k\right| \frac{\Delta t}{\Delta x} - c_{ij}\sin\theta_k \frac{\Delta t}{\Delta y}\right) f_{ijk} \\ &\quad + c_{ij}\left|\cos\theta_k\right| \frac{\Delta t}{\Delta x} f_{i+1,jk} + c_{ij}\sin\theta_k \frac{\Delta t}{\Delta y} f_{i,j-1,k}. \end{aligned} \tag{3.14}$$

  4) $\cos\theta_k < 0, \sin\theta_k < 0$

$$\begin{aligned} f_{ijk}^{n+1} &= \left(1 - c_{ij}\left|\cos\theta_k\right| \frac{\Delta t}{\Delta x} - c_{ij}\left|\sin\theta_k\right| \frac{\Delta t}{\Delta y}\right) f_{ijk} \\ &\quad + c_{ij}\left|\cos\theta_k\right| \frac{\Delta t}{\Delta x} f_{i+1,jk} + c_{ij}\left|\sin\theta_k\right| \frac{\Delta t}{\Delta y} f_{i,j+1,k}, \end{aligned} \tag{3.15}$$

where $0 \leq d_{k,k'} \leq 1$ and $d_{k,k'} + d_{k,k'+1} = 1$. We omit the superscript n of f_{ijk} on the right hand side.

Using the triangle inequality in (3.6)-(3.15), one typically gets the following

$$|f^{n+1}|_1 \leq \frac{1}{N_d} \sum_{(i,j,k)\in E_d} \alpha_{ijk} |f_{ijk}^n|, \tag{3.16}$$

where the coefficients α_{ijk} are positive. One can check that, under the hyperbolic CFL condition (3.4), $\alpha_{ijk} \leq 1$ except for possibly $(i,j,k) \in D_m \cup D_{m+1}$ with the definitions:

$$\begin{aligned} D_m &= \left\{ (m,j,k) \middle| \cos\theta_k > 0 \right\}, \\ D_{m+1} &= \left\{ (m+1,j,k) \middle| \cos\theta_k < 0,\ \left(\sin\left(|\theta_k| + \Delta\theta\right) \frac{C^-}{C^+} \right) < 1 \right\}. \end{aligned}$$

Denote

$$M_1 = \max_{(i,j,k)\in D_m} \alpha_{ijk}, \quad M_2 = \max_{(i,j,k)\in D_{m+1}} \alpha_{ijk}.$$

Our next step is to prove that M_1, M_2 are bounded independent of the mesh size. Let us first examine M_1.

Define the set

$$S_k^m = \left\{ k' \middle| \left(|\sin\theta_{k'}| \frac{c^-}{c^+} \right) < 1, \sin\theta_k \sin\theta_{k'} \geq 0, \cos\theta_{k'} > 0, |F_1(\theta_{k'}) - \theta_k| < \Delta\theta \right\} \quad \text{for } (m,j,k) \in D_m$$

with the function $F_1(\theta_{k'})$ given by

$$F_1(\theta_{k'}) = \begin{cases} \arcsin\left(|\sin\theta_{k'}| \frac{c^-}{c^+} \right) & \sin\theta_{k'} \geq 0 \\ -\arcsin\left(|\sin\theta_{k'}| \frac{c^-}{c^+} \right) & \sin\theta_{k'} < 0 \end{cases}.$$

Let the number of elements in S_k^m be N_k^m. One can check that $N_k^m \leq 2$ because every two elements $k_1', k_2' \in S_k^m$ satisfy $\left|F_1(\theta_{k_1'}) - F_1(\theta_{k_2'})\right| \geq |\theta_{k_1'} - \theta_{k_2'}| \frac{c^-}{c^+} > \Delta\theta$.

On the other hand, one can easily check from (3.6) and (3.8), for $(m,j,k) \in D_m$,

$$\alpha_{mjk} < 1 + N_k^m \leq 3,$$

so the boundedness of M_1 is proved.

Next we study M_2. Define the set

$$S_k^{m+1} = \left\{ k' \middle| \sin\theta_k \sin\theta_{k'} \geq 0, \cos\theta_{k'} < 0, |F_2(\theta_{k'}) - \theta_k| < \Delta\theta \right\} \quad \text{for } (m+1,j,k) \in D_{m+1}$$

with the function $F_2(\theta_{k'})$ given by

$$F_2(\theta_{k'}) = \begin{cases} \pi - \arcsin\left(|\sin\theta_{k'}| \frac{c^+}{c^-} \right) & \sin\theta_{k'} \geq 0 \\ -\pi + \arcsin\left(|\sin\theta_{k'}| \frac{c^+}{c^-} \right) & \sin\theta_{k'} < 0 \end{cases}.$$

From (3.10) and (3.11) one can get, for $(m+1,j,k) \in D_{m+1}$, the estimate for $\alpha_{m+1,jk}$:

$$\alpha_{m+1,jk} < 1 + \sum_{k' \in S_k^{m+1}} |\cos\theta_{k'}|. \tag{3.17}$$

The sequence $\theta_{k'}$, for $k' \in S_k^{m+1}$, composes an arithmetic progression with increment $\Delta\theta$. Denote the minimum and maximum elements in S_k^{m+1} by m_1, m_2 respectively. The summation in (3.17) can be estimated as

$$\sum_{k' \in S_k^{m+1}} |\cos\theta_{k'}| \quad < \quad 1 + \frac{1}{\Delta\theta} \left| \int_{\theta_{m_1}}^{\theta_{m_2}} \cos\theta d\theta \right|$$

$$
\begin{aligned}
&= 1 + \frac{1}{\Delta\theta} \left|\sin\theta_{m_2} - \sin\theta_{m_1}\right| \\
&= 1 + \frac{1}{\Delta\theta} \left|\sin\left(F_2(\theta_{m_2})\right) - \sin\left(F_2(\theta_{m_1})\right)\right| \frac{c^-}{c^+} \\
&\leq 1 + \frac{1}{\Delta\theta} \left|F_2(\theta_{m_2}) - F_2(\theta_{m_1})\right| \frac{c^-}{c^+} < 1 + 2\frac{c^-}{c^+}. \qquad (3.18)
\end{aligned}
$$

Combine (3.17) and (3.18), one gets

$$\alpha_{m+1,jk} < 2 + 2\frac{c^-}{c^+}$$

with $(m+1, j, k) \in D_{m+1}$. Therefore the boundedness of M_2 is proved.

In summary, we have

$$M_1 < 3, \quad M_2 < 2 + 2\frac{c^-}{c^+},$$

both are bounded independent of the mesh size.

Denote $M_1' = \max(0, M_1 - 1), M_2' = \max(0, M_2 - 1)$. From (3.16),

$$|f^{n+1}|_1 \leq |f^n|_1 + \frac{M_1'}{N_d} \sum_{(i,j,k)\in D_m} |f_{ijk}^n| + \frac{M_2'}{N_d} \sum_{(i,j,k)\in D_{m+1}} |f_{ijk}^n| \,. \qquad (3.19)$$

We now impose an assumption:

Assumption 1

There exists a constant $\theta_z \in (0, \frac{\pi}{2})$ such that

$$\forall (i,j,k) \in S_z = \{(i,j,k) | \;\; x_i < x_{m+\frac{1}{2}}, \;\; \frac{\pi}{2} - \theta_z < |\theta_k| < \frac{\pi}{2}\}, \qquad (3.20)$$

it holds that

$$|f_{ijk}^0| \leq C_1 |f^0|_1 \,. \qquad (3.21)$$

Remark: In the level set method [33, 7] for computing multivalued wave fronts, one typically solves the reduced Liouville equation with continuous initial values, for which Assumption 1 is satisfied. Thus our scheme should be suitable for such problems. It is also possible to construct a counter example which shows that the violation of this assumption leads to an unbounded numerical solution. Such a situation is similar to that for the finite difference version of the Hamiltonian preserving scheme for the Liouville equation with discontinuous potentials [25, 28]. One counter example will be given in Theorem 3.2.

We now establish the following theorem:

Theorem 3.1. *Under Assumption 1 and the CFL condition (3.4), scheme (3.6)-(3.15) is l^1-stable*

$$|f^L|_1 \leq C |f^0|_1.$$

Proof. From (3.19),

$$|f^L|_1 \le |f^0|_1 + \frac{M_1'}{N_d}\sum_{n=0}^{L-1}\left\{\sum_{(i,j,k)\in D_m}|f_{ijk}^n|\right\} + \frac{M_2'}{N_d}\sum_{n=0}^{L-1}\left\{\sum_{(i,j,k)\in D_{m+1}}|f_{ijk}^n|\right\}. \quad (3.22)$$

It remains to estimate

$$S_1 = \sum_{n=0}^{L-1}\left\{\sum_{(i,j,k)\in D_m}|f_{ijk}^n|\right\} \quad (3.23)$$

and

$$S_2 = \sum_{n=0}^{L-1}\left\{\sum_{(i,j,k)\in D_{m+1}}|f_{ijk}^n|\right\}. \quad (3.24)$$

We begin with estimating S_2.

Define the set

$$S_r = \{(i,j,k)|\ \ x_i > x_{m+\frac{1}{2}}, (m+1,j,k)\in D_{m+1}\}.$$

For all $(i,j,k)\in S_r$, due to the zero boundary condition and the upwind nature of the scheme, one has

$$f_{ijk}^n = \sum_{(p,q,r)\in S_r}\beta_{pqr}^{ijkn0} f_{pqr}^0, \quad (i,j,k)\in S_r \quad (3.25)$$

with $\beta_{pqr}^{ijkn0}\ge 0$.

Notice $D_{m+1}\subset S_r$,

$$S_2 \le \sum_{(p,q,r)\in S_r}\left(\sum_{n=0}^{L-1}\sum_{(i,j,k)\in D_{m+1}}\beta_{pqr}^{ijkn0}\right)|f_{pqr}^0| \equiv \sum_{(p,q,r)\in S_r}F(p,q,r)|f_{pqr}^0|, \quad (3.26)$$

where we have defined

$$F(p,q,r) \ = \ \sum_{n=0}^{L-1}\sum_{(i,j,k)\in D_{m+1}}\beta_{pqr}^{ijkn0}, \quad (p,q,r)\in S_r. \quad (3.27)$$

The next step is to estimate these coefficients. Define

$$\beta_{pqr}^{ijk0} = \sum_{n=0}^{\infty}\beta_{pqr}^{ijkn0}, \quad (p,q,r)\in S_r,$$

then (3.27) gives

$$F(p,q,r) = \sum_{(i,j,k)\in D_{m+1}} \sum_{n=0}^{L-1} \beta_{pqr}^{ijkn0} \le \sum_{(i,j,k)\in D_{m+1}} \beta_{pqr}^{ijk0}.$$

Hence it is useful to evaluate β_{pqr}^{ijk0}.

Notice β_{pqr}^{ijk0} is not zero only when $p \ge i$ and $r = k$ due to the upwind flux and constant wave speed. We first evaluate $\sum_j \beta_{pqr}^{ijk0}$ when $p = i$ and $r = k$ for $(i,j,k) \in S_r$. Denote $c_1^k = 1 - c^+ |\cos\theta_k| \frac{\Delta t}{\Delta x} - c^+ |\sin\theta_k| \frac{\Delta t}{\Delta y}$, $c_2^k = c^+ |\cos\theta_k| \frac{\Delta t}{\Delta x}$, $c_3^k = c^+ |\sin\theta_k| \frac{\Delta t}{\Delta y}$. Direct computation from scheme (3.14) or (3.15) gives

$$\beta_{iqk}^{iqk0} = \sum_{n=0}^{\infty} \beta_{iqk}^{iqkn0} = \sum_{n=0}^{\infty} (c_1^k)^n = \frac{1}{1-c_1^k} = \frac{1}{c_2^k + c_3^k}, \quad (i,q,k) \in S_r. \tag{3.28}$$

On the other hand, from scheme (3.14) and (3.15), for $(i,j,k) \in S_r$, $p \ge i$,

$$\beta_{pqk}^{ijk,n+1,0} = c_1^k \beta_{pqk}^{ijk,n,0} + c_2^k \beta_{pqk}^{i+1,jk,n,0} + c_3^k \beta_{pqk}^{i,j-1,k,n,0}, \qquad \sin\theta_k \ge 0, \tag{3.29}$$

$$\beta_{pqk}^{ijk,n+1,0} = c_1^k \beta_{pqk}^{ijk,n,0} + c_2^k \beta_{pqk}^{i+1,jk,n,0} + c_3^k \beta_{pqk}^{i,j+1,k,n,0}, \qquad \sin\theta_k < 0. \tag{3.30}$$

Take the situation $\sin\theta_k \ge 0$ for example. In (3.29), choose $p = i$ and take a summation for n from 0 to ∞ gives

$$\beta_{iqk}^{ijk0} = \frac{c_3^k}{c_2^k + c_3^k} \beta_{iqk}^{i,j-1,k0}, \quad j > q. \tag{3.31}$$

Combining (3.28) and (3.31) with the fact $\beta_{iqk}^{ijk0} = 0$ for $j < q$, one gets

$$\sum_j \beta_{iqk}^{ijk0} < \frac{1}{c_2^k} < \frac{1}{c^+ \cos\left(\arcsin\left(\frac{c^+}{c^-}\right) + \Delta\theta\right)} \frac{\Delta x}{\Delta t} \equiv \lambda_1, \quad (i,j,k) \in S_r.$$

The situation $\sin\theta_k < 0$ leads to the same conclusion.

We now evaluate $\sum_j \beta_{pqr}^{ijk0}$ when $p > i$ and $r = k$ for $(i,j,k) \in S_r$. Summing up j in (3.29) or (3.30) gives

$$\sum_j \beta_{pqk}^{ijk,n+1,0} \le (c_1^k + c_3^k) \sum_j \beta_{pqk}^{ijk,n,0} + c_2^k \sum_j \beta_{pqk}^{i+1,jk,n,0}, \tag{3.32}$$

then a sum of n from 0 to ∞ in (3.32) gives

$$\sum_j \beta_{pqk}^{ijk0} \le \sum_j \beta_{pqk}^{i+1,jk0}, \quad i < p. \tag{3.33}$$

We now evaluate $F(p,q,r)$ for $(p,q,r) \in S_r$,

$$F(p,q,r) \leq \sum_{(i,j,k)\in D_{m+1}} \beta_{pqr}^{ijk0} = \sum_j \beta_{pqr}^{m+1,jr0} \leq \sum_j \beta_{pqr}^{m+2,jr0} \leq \cdots \leq \sum_j \beta_{pqr}^{pjr0} < \lambda_1. \tag{3.34}$$

Therefore, from (3.26) one gets

$$\begin{aligned} S_2 &\leq \sum_{(p,q,r)\in S_r} F(p,q,r)|f_{pqr}^0| < \lambda_1 \sum_{(p,q,r)\in S_r} |f_{pqr}^0| \\ &\leq \lambda_1 \sum_{(p,q,r)\in E_d} |f_{pqr}^0| = \lambda_1 N_d |f^0|_1. \end{aligned} \tag{3.35}$$

Our next step is to estimate S_1. Define the set

$$S_l = \{(i,j,k)|\ \ x_i < x_{m+\frac{1}{2}}, (m,j,k) \in D_m\}.$$

Similarly when $(i,j,k) \in S_l$, one has

$$f_{ij}^n = \sum_{(p,q,r)\in S_l} \gamma_{pqr}^{ijkn0} f_{pqr}^0, \quad (i,j,k) \in S_l. \tag{3.36}$$

Dividing set D_m into two parts:

$$D_m^1 = \left\{(i,j,k) \in D_m \middle| |\theta_k| \leq \frac{\pi}{2} - \theta_z \right\}, \quad D_m^2 = \left\{(i,j,k) \in D_m \middle| |\theta_k| > \frac{\pi}{2} - \theta_z \right\},$$

and also define the corresponding two parts of S_l

$$S_l^1 = \left\{(i,j,k) \in S_l \middle| |\theta_k| \leq \frac{\pi}{2} - \theta_z \right\}, \quad S_l^2 = \left\{(i,j,k) \in S_l \middle| |\theta_k| > \frac{\pi}{2} - \theta_z \right\}.$$

Note that S_l^2 is a subset of S_z in (3.20).

Correspondingly, S_1 is also divided into two parts

$$S_1 = \sum_{n=0}^{L-1} \left\{ \sum_{(i,j,k)\in D_m^1} |f_{ijk}^n| \right\} + \sum_{n=0}^{L-1} \left\{ \sum_{(i,j,k)\in D_m^2} |f_{ijk}^n| \right\} = S_{11} + S_{12}. \tag{3.37}$$

Similar to the previous case, one can get the upper bound for the first term

$$S_{11} < \lambda_2 N_d |f^0|_1 \tag{3.38}$$

with $\lambda_2 \equiv \frac{1}{c^- \sin\theta_z} \frac{\Delta x}{\Delta t}$. Substituting (3.36) into S_{12} gives

$$S_{12} \leq \sum_{(p,q,r)\in S_l^2} \left(\sum_{n=0}^{L-1} \sum_{(i,j,k)\in D_m^2} \gamma_{pqr}^{ijkn0} \right) |f_{pqr}^0|.$$

Using Assumption 1,

$$\begin{aligned} S_{12} &\leq C_1|f^0|_1 \sum_{(p,q,r)\in S_l^2} \left(\sum_{n=0}^{L-1} \sum_{(i,j,k)\in D_m^2} \gamma_{pqr}^{ijkn0} \right) \\ &= C_1|f^0|_1 \sum_{n=0}^{L-1} \sum_{(i,j,k)\in D_m^2} \left(\sum_{(p,q,r)\in S_l^2} \gamma_{pqr}^{ijkn0} \right). \end{aligned} \tag{3.39}$$

Now we evaluate $\sum_{(p,q,r)\in S_l^2} \gamma_{pqr}^{ijkn0}$ when $(i,j,k) \in D_m^2$. Write (3.36) as

$$f_{ijk}^n = \sum_{(p,q,r)\in S_l^2} \gamma_{pqr}^{ijkn0} f_{pqr}^0, \quad (i,j,k) \in D_m^2. \tag{3.40}$$

When the initial value of f is a constant, even at the ghost cells, the numerical solutions at the next time step will be the same constant, while the coefficients γ_{pqr}^{ijkn0} in (3.40) do not include those corresponding to the ghost cells, thus

$$\sum_{(p,q,r)\in S_l^2} \gamma_{pqr}^{ijkn0} \leq 1, \quad \forall (i,j,k) \in D_m^2.$$

Continuing from (3.39),

$$\begin{aligned} S_{12} &\leq C_1|f^0|_1 \sum_{n=0}^{L-1} \sum_{(i,j,k)\in D_m^2} 1 \leq \frac{C_1|f^0|_1 L N_d}{N} \\ &= \frac{C_1 T N_d}{(x_{N+\frac{1}{2}} - x_{\frac{1}{2}})} \frac{\Delta x}{\Delta t} |f^0|_1 \equiv \lambda_3 N_d |f^0|_1 \end{aligned} \tag{3.41}$$

with $\lambda_3 = \frac{C_1 T}{(x_{N+\frac{1}{2}} - x_{\frac{1}{2}})} \frac{\Delta x}{\Delta t}$ being an $O(1)$ quantity.

Now from (3.37), (3.38) and (3.41),

$$S_1 < (\lambda_2 + \lambda_3) N_d |f^0|_1. \tag{3.42}$$

Combining (3.22), (3.35) and (3.42),

$$\begin{aligned} |f^L|_1 &< |f^0|_1 + M_1' \lambda_1 |f^0|_1 + M_2' (\lambda_2 + \lambda_3) |f^0|_1 \\ &= [1 + M_1' \lambda_1 + M_2' (\lambda_2 + \lambda_3)] |f^0|_1 \\ &\equiv C |f^0|_1 \end{aligned}$$

where $C \equiv 1 + M_1' \lambda_1 + M_2' (\lambda_2 + \lambda_3)$. Thus Theorem 3.1 is proved. □

There do exist counter examples which violate Assumption 1 and lead to unbounded numerical solutions. For example, let k_0 be the index such that $\theta_{k_0} < \theta_{k_0+1} < \arcsin\left(\frac{c^+}{c^-}\right) \le \theta_{k_0+2}$. Denote $\theta^- = \arcsin\left(\sin(\theta_{k_0})\frac{c^-}{c^+}\right)$. Assume $\theta_{k'} \le \theta^- < \theta_{k'+1} < \frac{\pi}{2}$. Define

$$k'' = \begin{cases} k' & \frac{\theta_{k'+1}-\theta^-}{\Delta\theta} \ge \frac{1}{2} \\ k'+1 & \frac{\theta_{k'+1}-\theta^-}{\Delta\theta} < \frac{1}{2} \end{cases} .$$

choose the initial data as

$$f^0_{ijk} = \begin{cases} 1 & i = m, j = 1, k = k'' \\ 0 & \text{else} \end{cases} . \tag{3.43}$$

We consider the case that $L < M$ and $L < N - m$ so that the nonzero part of the numerical solution has not reached the domain boundary at $t = T$. In such a situation, we have

Theorem 3.2. *Under the CFL condition (3.4), the scheme (3.6)-(3.15) with the initial data (3.43) and the zero boundary condition is l^1-unstable*

$$|f^L|_1 > B|f^0|_1,$$

where

$$B = 1 + \left(\frac{c^+}{2}\frac{\Delta t}{\Delta x}\cos\theta_{k_0} - c^-\frac{\Delta t}{\Delta x}\cos\widehat{\theta}_1\right)\frac{1-(1-c^-\frac{\Delta t}{\Delta x}\cos\widehat{\theta}_2)^L}{c^-\frac{\Delta t}{\Delta x}\cos\widehat{\theta}_1}$$

with

$$\begin{aligned} \widehat{\theta}_1 &= \arcsin\left(\sin\left[\arcsin\left(\frac{c^+}{c^-}\right) - 2\Delta\theta\right]\frac{c^-}{c^+}\right) - \frac{\Delta\theta}{2}, \\ \widehat{\theta}_2 &= \arcsin\left(\sin\left[\arcsin\left(\frac{c^+}{c^-}\right) - \Delta\theta\right]\frac{c^-}{c^+}\right) + \frac{\Delta\theta}{2}. \end{aligned}$$

The coefficient B tends to ∞ as the mesh size goes to zero.

The proof for Theorem 3.2 can be carried out by using similar analysis adopted in the proof for Theorem 3.1 and is omitted in this paper.

4 Numerical examples

In this section we present numerical examples to show the deficiency of the SFDM for the reduced Liouville equation with discontinuous wave speeds and to demonstrate the validity and study the numerical accuracy of the proposed scheme. In the numerical computations the second order TVD Runge-Kutta time discretization

[40] is used, while for space the second order flux, described at the end of Section 3.1, is used with $D_c = 1.1$. The exact solution is obtained using the method of characteristics.

Example 4.1. A piecewise constant wave speed problem with only wave transmission at an interface. This is an example from [33]. Consider the reduced Liouville equation (1.1) with a piecewise constant local wave speed given by

$$c(x,y) = \begin{cases} 2, & x < 0, \\ 1, & x > 0. \end{cases}$$

The initial wave front is a circle centered at $(-0.5, 0)$ with radius 0.2 and the wave direction is the outward normal of the circle. As done in [33, 7], the initial values of the two level set functions can be chosen as

$$\phi(x,y,\theta,0) = x + 0.5 - 0.2\cos\theta, \quad \psi(x,y,\theta,0) = y - 0.2\sin\theta.$$

These level set functions are evolved according to the reduced Liouville equation (1.1). The common zero level sets of ϕ and ψ give the wave front.

The computational domain in this example is $(x,y,\theta) \in [-1,1]\times[-1,1]\times(-\pi,\pi]$. We compare the 2nd order SFDM by either ignoring (SFDMI) or smoothing out (SFDMS) the wave speed discontinuities with the new scheme developed in this paper for the 2D reduced Liouville equation (1.1) to solve the level set functions ϕ and ψ. The wave fronts are plotted out by finding the common zero points of ϕ and ψ in each cube in the reduced phase space formed by grid points by the linear interpolation process. Since the solutions are discontinuous at the interface $x = 0$, we need special treatment in the cube intersecting with the interface. In such a cube, we divide this cube into two cubes separated by the plane $x = 0$, and find the common zero points of ϕ and ψ in each of the two cubes respectively. The left and right limit values of ϕ and ψ at plane $x = 0$ are interpolated from their values at each side of the plane.

In the computation, the time step is chosen as $\Delta t = \frac{1}{3}\Delta x$ for the new scheme and the SFDMI. In the SFDMS, we replace the wave speed discontinuities by a linear function connecting the two limit constants across a transition zone that contains a few mesh cells. Since the gradient of the smoothed wave speed across the transition zone increases with mesh refinement, the SFDMS is subject to a more severe CFL condition than a hyperbolic CFL condition required by the new scheme. Fig. 4.1-4.3 show respectively the numerical wave fronts with wave directions at $t = 0$ and $t = 0.3$ by the three methods on the $50^2 \times 52$ mesh along with the exact wave front. We used 5 cells for the transition zone in the SFDMS. The exact wave front at $t = 0.3$ in this example is given by

$$\begin{cases} x = 0.8\cos\theta - 0.5,\ y = 0.8\sin\theta, & \theta \in (-\pi, -\theta_0) \cup (\theta_0, \pi] \\ x = \frac{\cos\theta}{2}\left(0.8 - \frac{0.5}{\sqrt{1-4\sin\theta^2}}\right), & \\ y = 1.6\sin\theta - \frac{3\sin\theta}{2}\left(0.8 - \frac{0.5}{\sqrt{1-4\sin\theta^2}}\right), & \theta \in (-\theta_1, \theta_1) \end{cases} \tag{4.1}$$

with $\theta_0 = \arccos\left(\frac{5}{8}\right), \theta_1 = \arcsin\left(\frac{\sin\theta}{2}\right)$.

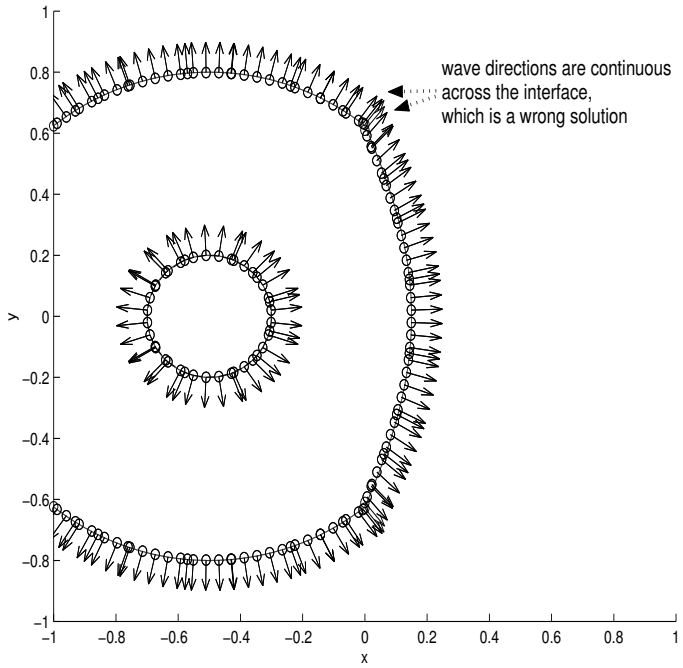

Figure 4.1 Example 4.1, Wave front with wave directions at $t = 0$ and $t = 0.3$. Solid line: exact wave front; 'o': computed wave front by the SFDMI using the $50^2 \times 52$ mesh; arrow: numerical wave directions.

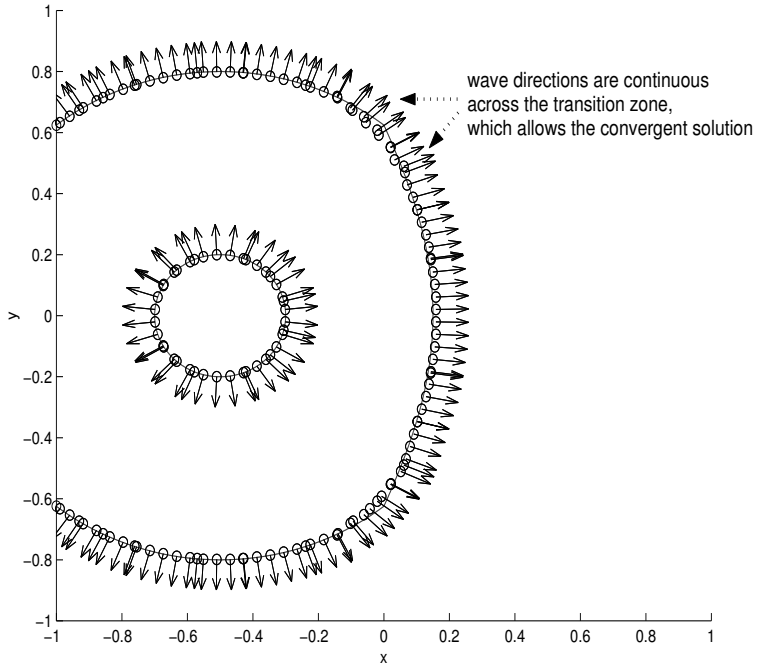

Figure 4.2 Example 4.1, Wave front with wave directions at $t = 0$ and $t = 0.3$. Solid line: exact wave front; 'o': numerical wave front by the SFDMS using the $50^2 \times 52$ mesh; arrow: numerical wave directions.

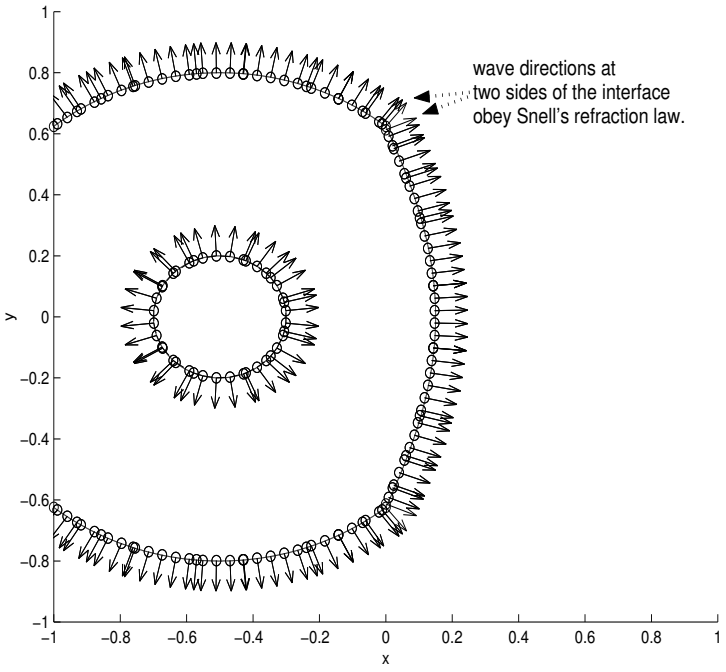

Figure 4.3 Example 4.1, Wave front with wave directions at $t = 0$ and $t = 0.3$. Solid line: exact wave front; 'o': numerical wave front by the new scheme using the $50^2 \times 52$ mesh; arrow: numerical wave directions.

Although the numerical wave front by the SFDMI is close to the correct solution, from the numerical wave directions it can be observed that the SFDMI gives wrong wave directions at the right hand side of the interface. In fact, the SFDMI selects out the solution where the particle does not change direction when passing through the interface. This is not the physically relevant solution. Thus although the SFDMI does not suffer from a more severe CFL condition than a hyperbolic one, it gives a wrong wave front since the numerical wave directions are wrong. In comparison, the new scheme and the SFDMS give correct transmissions satisfying Snell's Law through the interface.

Table 4.1 presents the averaged distance (AD) from the numerical wave front to the exact wave front on the right hand side of the interface $x > 0$ by the SFDMI with different meshes. These results exhibit a non-convergence, agreeing with our analysis above. Table 4.2 presents the AD on the whole computational domain in the physical space by the SFDMS with different meshes. The transition zone width is set to be $5\Delta x, 9\Delta x$ and $11\Delta x$ respectively for the three meshes, which is proportional to the square root of the mesh size with mesh refinement to enforces the convergence of the numerical solutions. The CFL condition for the method becomes more severe with the mesh refinement. From the results we observe that the solutions are only of halfth order accuracy due to the regularization of the discontinuous wave speed. Thus the SFDMS is not an economic method for dealing with a discontinuous wave speed problem. Table 4.3 presents the AD on the full physical space by the new scheme with different meshes. These results show the second order accuracy of the

numerical wave front.

Table 4.1 The AD on $x > 0$ by the SFDMI with different meshes

grid points	$26^2 \times 28$	$50^2 \times 52$	100^3	200^3
	7.9060E-3	3.9266E-3	3.0063E-3	2.6753E-3

Table 4.2 The AD on the entire computational domain in the physical space by the SFDMS with different meshes

grid points	$50^2 \times 52$	100^3	200^3
AD	5.1540E-3	3.5967E-3	2.2705E-3
$\frac{\Delta t}{\Delta x}$	1/8	1/10	1/14

Table 4.3 The AD on the entire computational domain in the physical space by the new scheme with different meshes

grid points	$50^2 \times 52$	100^3	200^3
	1.8597E-3	4.4134E-4	1.0330E-4

Example 4.2. A piecewise constant wave speed problem with wave transmission and reflection at an interface. This problem is a slight modification of Example 4.1. Let

$$c(x,y) = \begin{cases} 1, & x < 0, \\ 2, & x > 0, \end{cases}$$

The initial wave front forms a circle centered at $(-0.5, 0)$ with radius 0.4 and the wave direction is the outward normal of the circle. The initial values of the two level set functions are chosen to be

$$\phi(x,y,\theta,0) = x + 0.5 - 0.4\cos\theta, \quad \psi(x,y,\theta,0) = y - 0.4\sin\theta.$$

The computational domain in this example is $(x,y,\theta) \in [-1,1]\times[-1,1]\times(-\pi,\pi]$. The time step is chosen as $\Delta t = \frac{1}{3}\Delta x$ for the new scheme and the SFDMI. We first show the initial wave front at $t = 0$, the exact and numerical wave fronts with wave directions by the SFDMI at $t = 0.5$ in Fig. 4.4. The exact wave front at $t = 0.5$ is

given by

$$\begin{cases} x = 0.9\cos\theta - 0.5,\ y = 0.9\sin\theta, & \theta \in (-\pi, -\theta_0) \cup (\theta_0, \pi] \\ x = 0.9\cos\theta + 0.5,\ y = 0.9\sin\theta, & \theta \in (-\frac{5}{6}\pi, -\pi + \theta_0) \cup (\pi - \theta_0, \frac{5}{6}\pi) \\ x = 2\cos\theta\left(0.9 - \frac{0.5}{\sqrt{1-\frac{1}{4}\sin\theta^2}}\right), & \\ y = 0.45\sin\theta + \frac{3\sin\theta}{2}\left(0.9 - \frac{0.5}{\sqrt{1-\frac{1}{4}\sin\theta^2}}\right), & \theta \in (-\frac{\pi}{2}, \frac{\pi}{2}) \end{cases} \tag{4.2}$$

with $\theta_0 = \arccos\left(\frac{5}{9}\right)$.

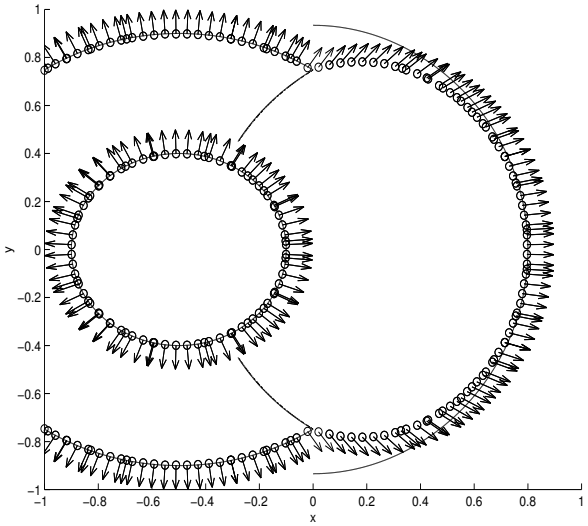

Figure 4.4 Example 4.2, Wave front with wave directions at $t = 0$ and $t = 0.5$. Solid line: exact wave front; 'o': numerical wave front by the SFDMI using $50^2 \times 52$ mesh; arrows: numerical wave directions.

From Fig. 4.4 it can be seen that the SFDMI gives wrong wave fronts by incorrectly dealing with the transmission wave velocity as well as not taking into account the reflection wave at the interface.

Next we present the results by the SFDMS. Fig. 4.5 depicts the numerical wave fronts at $t = 0.5$ by the SFDMS with the 200^3 mesh with different transition zone widths along with the exact wave front. It can be observed that even by using such a fine mesh, the reflection wave fronts are not accurately approximated in both cases, although the results by using smaller transition zone widths are more accurate. These results indicate that the more accurate reflection wave front can only be obtained by the SFDMS using a much smaller transition zone width. Thus one needs to use a much finer mesh, since it is needed to put enough grid points in the transition zone to ensure the convergence of the SFDMS. The smaller transition zone width also causes a much more severe CFL condition, due to the increase of the derivative of the smoothed c.

One can also observe that some spurious wave fronts connecting the correct wave fronts appear in these results. This is due to the plotting procedure, which can be fixed by a post-processing plotting filter to be elaborated next when we discuss the results of the new scheme.

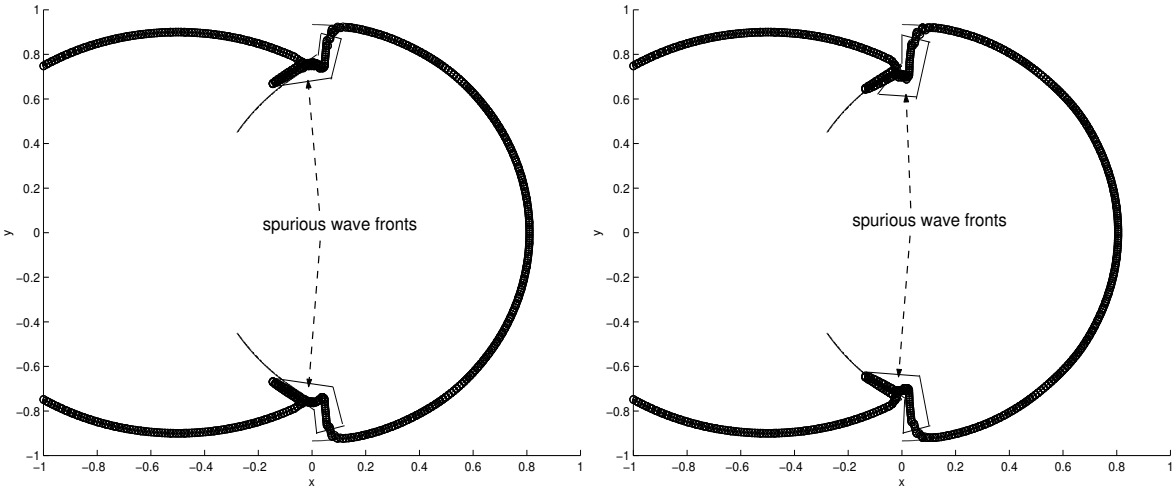

Figure 4.5 Example 4.2, Wave front at $t = 0.5$. Solid line: exact wave front; 'o': numerical wave front by the SFDMS using the 200^3 mesh. Left: transition zone width being $9\Delta x$, $\frac{\Delta t}{\Delta x} = 1/15$; Right: transition zone width being $5\Delta x$, $\frac{\Delta t}{\Delta x} = 1/24$.

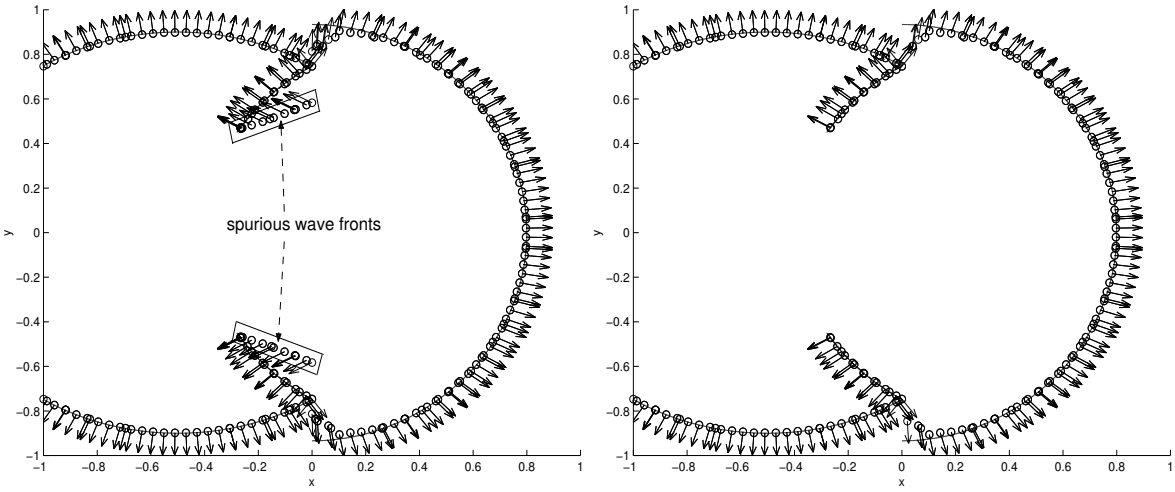

Figure 4.6 Example 4.2, Wave front with wave directions at $t = 0.5$. Solid line: exact wave front; 'o': numerical wave front by the new scheme using the $50^2 \times 52$ mesh; arrows: numerical wave directions. Left: spurious wave fronts arise without using the plotting filter; Right: spurious wave fronts removed with the plotting filter.

We then present the results by the new scheme. The left part in Fig. 4.6 shows the numerical wave front with wave directions at $t = 0.5$ by the new scheme on the

$50^2 \times 52$ mesh along with the exact wave front. The new scheme correctly captures the wave transmission and reflection at the interface. Note that similar spurious wave fronts as those by the SFDMS also arise. These spurious wave fronts are produced due to the discontinuities of the level set functions ϕ and ψ whose values have opposite signs on both sides of the interface, and the graphic plotter takes the value in between as zero. Such discontinuities arise from the fact that the wave may be transmitted or reflected by different incident angles. The fronts so plotted do not correspond to the true common zero points of the level set functions. Note such discontinuities do not appear in the level set functions when dealing with a complete reflection at a boundary, in which case the wave fronts may remain smooth [7].

To remove such spurious fronts, we can implement a filter process in the plotting procedure. When finding the common zero points of ϕ and ψ in a cube, we check their values in this cube. If the difference between the maximum value and the minimum values in the cube is larger than a value C_d, then we assume there are discontinuities of ϕ and ψ in this cube and do not find the common zeroes in this cube. The parameter C_d should not be too small in order to prevent the correct wave fronts from being mistakenly ignored by this filter. In this example we choose $C_d = (\Delta x)^{\frac{1}{10}}$. The right part in Fig. 4.6 shows the exact wave front and the filtered numerical wave front with wave directions at $t = 0.5$ by the new scheme on $50^2 \times 52$ mesh. The spurious wave fronts are no longer there.

We notice that we did not use this filter process in the computation of Example 4.1. For a general problem, one does not know whether the filter process is needed before computation. So one can just apply the filter in any case. In the usual situation that the level set functions are smooth near their common zero points or the wave fronts, using this filter does not filter out the correct wave front if the computational mesh is reasonably fine. In example 4.1, the use of this filter with parameter $C_d = (\Delta x)^{\frac{1}{10}}$ will produce exactly the same results as those given in Table 4.3.

There are also discontinuities in ϕ and ψ on the right hand side of the interface due to wave transmission by the interface. These discontinuities are close to the common zero points of ϕ and ψ near the interface, which lead to an accuracy loss of the numerical wave fronts in the right hand neighborhood of the interface. Fig. 4.7 shows the exact wave front and the numerical wave fronts at $t = 0.5$ by the new scheme on different meshes (with the plotting filter added) plotted in an area near the interface. It can be seen that the numerical wave fronts have a lower accuracy in the right hand neighborhood of the interface, while the wave fronts at the left hand side of the interface, including the reflection wave front, are much more accurately resolved.

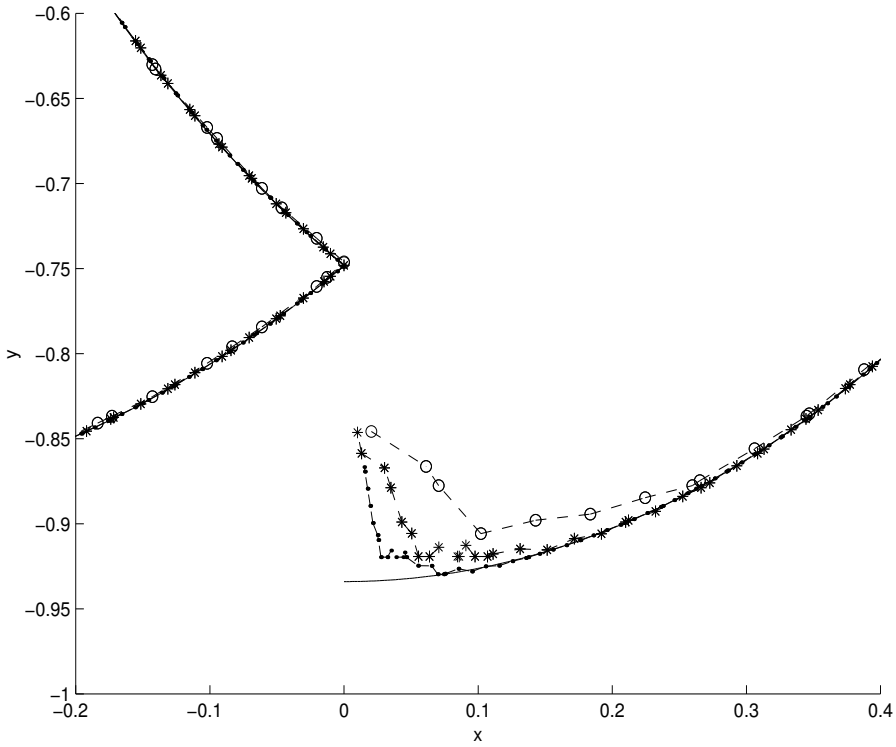

Figure 4.7 Example 4.2, Wave fronts at $t = 0.5$. Solid line: exact wave front; 'o': computed wave front by the new scheme using $50^2 \times 52$ mesh; '$*$': 100^3 mesh; '$\cdot$': 200^3 mesh.

Table 4.4 presents the AD on the entire computational domain in the physical space by the new scheme with different meshes (with the plotting filter added). It can be seen that the numerical wave fronts by the new scheme are of the first order accuracy, for the reason given above.

Table 4.4 AD by the new scheme with different meshes

grid points	$50^2 \times 52$	100^3	200^3
	4.0460E-3	2.1935E-3	8.3591E-4

5 Conclusion

We construct and study a new numerical scheme suitable for the reduced Liouville equation of geometrical optics with discontinuous local wave speeds in two space dimensional case. Such problems arise in geometrical optics with interfaces, where waves are fully transmitted or reflected, satisfying Snell's Law of Refraction. The

design principle is similar to our previous works [26, 27] for the Liouville equation in full space, in that we also build into numerical flux the wave behavior at the interface. Our new scheme is explicit, and allows a hyperbolic CFL condition, under which the scheme is proved to be positive, l^∞ contracting, and l^1 stable under a suitable assumption on the initial data. Numerical experiments are carried out to demonstrate its superiority over approaches that ignore the interface or smooth out the interface.

This new scheme corresponds to the finite difference version of the Hamiltonian-preserving scheme developed in [26]. The scheme corresponding to the finite volume version of the method in [26] can also be designed similarly, but will not be given here.

In the future we will consider more complex interfaces, along the line of [21], and the extension of our method for the general case of partial transmissions and reflections at the interface. The framework presented in this paper can also be used for the paraxial formulation (see for example [30]) in order to speed up the computation, and to compute the amplitude of the wave, which is an ongoing project by the authors.

References

[1] G. Bal, J.B. Keller, G. Papanicolaou and L. Ryzhik, Transport theory for acoustic waves with reflection and transmission at interfaces, Wave Motion, 30, 303-327 (1999).

[2] J.-D. Benamou, Big Ray Tracing: Multivalued Travel Time Field Computation Using Viscosity Solutions of the Eikonal Equation, J. Comput. Phys. 128, 463-474 (1996).

[3] J.-D. Benamou, Direct computation of multivalued phase space solutions for Hamilton-Jacobi equations, Comm. Pure Appl. Math. 52(11), 1443-1475 (1999).

[4] J.-D. Benamou, An introduction to Eulerian geometrical optics(1992-2002), J. Sci. Comp. 19(1-3), 63-93, Dec. (2001).

[5] J.-D. Benamou and I. Solliec, An Eulerian Method for Capturing Caustics, J. Comput. Phys. 162(1), 132-163 (2000).

[6] P. Burchard, L.-T. Cheng, B. Merriman and S. Osher, Motion of curves in three spatial dimensions using a level set approach, J. Comput. Phys. 170 (2001), no. 2, 720-741.

[7] Li-Tien Cheng, Myungjoo Kang, Stanley Osher, Hyeseon Shim, and Yen-Hsi Tsai, Reflection in a Level Set Framework for Geometric Optics , Computer Modeling in Engineering and Sciences 5, 347-360, 2004.

[8] L.-T. Cheng, H.-L. Liu and S. Osher, Computational high-frequency wave propagation using the Level Set method, with applications to the semi-classical limit of Schrödinger equations, Comm. Math. Sci. 1, 593-621, 2003.

[9] B. Cockburn, J. Qian, F. Reitich and J. Wang, An accurate spectral/discontinuous finite-element formulation of a phase space-based level set approach to geometrical optics, J. Comp. Phys. 208, 175-195, 2005.

[10] B. Engquist and O. Runborg, Multi-phase computations in geometrical optics, J. Comput. Appl. Math. 74, 175-192 (1996).

[11] B. Engquist and O. Runborg, Multiphase computations in geometrical optics, In M. Fey and R. Jeltsch, editors, Hyperbolic Problems: Theory, Numerics, Applications, volume 129 of Internat. Ser. Numer. Math., Zürich, Switzerland, 1998. ETH Zentrum.

[12] B. Engquist and O. Runborg, Computational high frequency wave propagation, Acta Numerica 12, 181-266 (2003).

[13] B. Engquist, O. Runborg and A.-K. Tornberg, High-Frequency Wave Propagation by the Segment Projection Method, J. Comput. Phys. 178(2), 373-390 (2002).

[14] B. Engquist, A.K. Tornberg and R. Tsai, Discretization of dirac delta functions in level set methods, J. Comp. Phys., to appear.

[15] E. Fatemi, B. Engquist and S. Osher, Numerical solution of the high frequency asymptotic expansion for the scalar wave equation, J. Comput. Phys. 120, 145-155 (1995).

[16] S. Fomel and J.A. Sethian, Fast Phase Space Computation of Multiple Arrivals, Proc. Natl. Acad. Sci. USA 99(11), 7329-7334 (2002).

[17] L. Gosse and F. James, Numerical approximations of one-dimensional linear conservation equations with discontinuous coefficients, Math. Comp. 987-1015, 2000.

[18] L. Gosse, Using K-branch entropy solutions for multivalued geom etric optics computations, J. Comp. Phys. 180, 155–182, 2002.

[19] L. Gosse, Multiphase semiclassical approximation of an electron in a one-dimensional crystalline lattice II. Impurities, confinement and Bloch oscillations, J. Comp. Phys. 201, 344-375, 2004.

[20] L. Gosse, S. Jin and X.T. Li, On Two Moment Systems for Computing Multiphase Semiclassical Limits of the Schrodinger Equation Math. Model Methods Appl. Sci. 13, 1689-1723, 2003.

[21] S. Jin and X. Liao, A Hamiltonian-preserving scheme for high frequency elastic waves in heterogeneous media, J. Hyperbolic Diff. Eqn., to appear.

[22] S. Jin, H.L. Liu, S. Osher and R. Tsai, Computing multivalued physical observables for the semiclassical limit of the Schrodinger equation, J. Comp. Phys. 205, 222-241 (2005).

[23] S. Jin, H.L. Liu, S. Osher and R. Tsai, Computing multi-valued physical observables for high frequency limit of symmetric hyperbolic systems, J. Comp. Phys. 210, 497-518 (2005).

[24] S. Jin and S. Osher, A level set method for the computation of multi-valued solutions to quasi-linear hyperbolic PDE's and Hamilton-Jacobi equations, Comm. Math. Sci. 1(3), 575-591 (2003).

[25] S. Jin and X. Wen, Hamiltonian-preserving schemes for the Liouville equation with discontinuous potentials, Commun. Math. Sci. 3, 285-315 (2005).

[26] S. Jin and X. Wen, Hamiltonian-preserving schemes for the Liouville equation of geometrical optics with discontinuous local wave speeds, J. Comput. Phys. 214, 672-697 (2006).

[27] S. Jin and X. Wen, A Hamiltonian-preserving scheme for the Liouville equation of geometrical optics with partial transmissions and reflections, SIAM J. Numer. Anal., to appear.

[28] S. Jin and X. Wen, The l^1-stability of a Hamiltonian-preserving scheme for the Liouville equation with discontinuous potentials, preprint.

[29] N.N. Kuznetsov, On stable methods for solving non-linear first order partial differential equations in the class of discontinuous functions, Topics in Numerical Analysis III (Proc. Roy. Irish Acad. Conf.)(J.J.H.Miller, ad.), Academic Press, London, 183-197 (1977).

[30] S.Y. Leung, J. Qian and S. Osher, A level set method for three-dimensional paraxial geometrical optics with multiple sources, Comm. Math. Sci. 2, 643-672, 2004.

[31] R.J. LeVeque, Numerical Methods for Conservation Laws, Birkhauser-Verlag, Basel, 1990.

[32] L. Miller, Refraction of high frequency waves density by sharp interfaces and semiclassical measures at the boundary, J. Math. Pures Appl. IX 79, 227-269, (2000).

[33] S. Osher, L.-T. Cheng, M. Kang, H. Shim and Y.-H. Tsai, Geometric optics in a phase-space-based level set and Eulerian framework, J. Comput. Phys. 179(2), 622-648 (2002).

[34] B. Perthame and C.W. Shu, On positivity preserving finite volume schemes for Euler equations, Numer. Math. 73, 119-130 (1996).

[35] B. Perthame and C. Simeoni, A kinetic scheme for the Saint-Venant system with a source term, CALCOLO 38(4), 201-231 (2001).

[36] J. Qian, L.-T. Cheng and S. Osher, A level set based Eulerian approach for anisotropic wave propagations, Wave Motion 37, 365-379, 2003.

[37] O. Runborg, Some new results in multiphase geometrical optics, M2AN Math. Model. Numer. Anal. 34, 1203-1231 (2000).

[38] L. Ryzhik, G. Papanicolaou and J. Keller, Transport equations for elastic and other waves in random media, Wave Motion 24, 327-370 DEC (1996).

[39] L. Ryzhik, G. Papanicolaou and J. Keller, Transport equations for waves in a half space, Comm. PDE's, 22, 1869-1910 (1997).

[40] C.W. Shu and S. Osher, Efficient implementation of essentially non-oscillatory shock capturing scheme, J. Comput. Phys. 77, 439-471 (1988).

[41] W. Symes and J. Qian, A slowness matching Eulerian method for multivalued solutions of Eikonal equations, J. Sci. Comp. 19(1-3), 501-526, (2003). Special issue in honor of the sixtieth birthday of Stanley Osher.

[42] P.K. Sweby, High-resolution schemes using flux limiters for hyperbolic conservation-laws, SIAM J. Num. Anal. 21, 995-1011, 1984.

[43] T. Tang and Z.H. Teng, The sharpness of Kuznetsov's $O(\sqrt{\Delta x})$ L^1-error estimate for monotone difference schemes, Math. Comp. 64, 581-589 (1995).